Tuning heat transport in trapped-ion chains across a structural phase transition

A. Ruiz,[1,2] D. Alonso,[1,2] M. B. Plenio,[3] and A. del Campo[4,5]
[1]*Departamento de Física, Universidad de La Laguna, La Laguna 38203, Spain*
[2]*IUdEA Instituto Universitario de Estudios Avanzados, Universidad de La Laguna, La Laguna 38203, Spain*
[3]*Institut für Theoretische Physik, Albert-Einstein-Allee 11, Universität Ulm, D-89069 Ulm, Germany*
[4]*Theoretical Division, Los Alamos National Laboratory, Los Alamos, New Mexico 87545, USA*
[5]*Center for Nonlinear Studies, Los Alamos National Laboratory, Los Alamos, New Mexico 87545, USA*
(Received 21 January 2014; revised manuscript received 24 May 2014; published 13 June 2014)

We analyze the heat transport in an ion chain that is confined in a strongly anisotropic Paul trap. To drive a heat current across the chain different pairs of counterpropagating laser beams are applied to the ions on the edges. The lasers behave as heat reservoirs operating at different temperatures, and a nonequilibrium heat flow can be sustained. The control of the spatial distribution of the ions in the chain by variation of the trapping frequencies makes ion chains an ideal testbed to study heat transport properties in finite open systems of low dimensionality with tunable nonlinearities. We explore heat transport across a structural phase transition between the linear and zigzag configurations, identifying the condition for optimal heat transport.

DOI: 10.1103/PhysRevB.89.214305 PACS number(s): 64.60.Ht, 05.60.−k, 05.70.Fh, 37.10.Ty

I. INTRODUCTION

Ultracold ion Coulomb crystals represent one of the most promising platforms for the simulation of many-body physics thanks to the high degree of spatial and temporal control of mesoscopic ion crystals they afford us [1–3]. Recent years have seen a shift away from the study of ground and thermal state properties, towards the exploration of the potential role of ion traps as a testbed for models of nonequilibrium statistical mechanics.

In this context it is important to recognize that, in addition to the electronic spin degrees of freedom, trapped ions also possess motional degrees of freedom that can exhibit highly nontrivial static and dynamical properties including classical and quantum phase transitions. Indeed, ion Coulomb crystals confined in ion traps may support a wide variety of phases including a linear chain and a doubly-degenerate zigzag phase, extending further to increasingly complex configurations in two and three spatial dimensions [4–6]. The associated structural phase transitions between those configurations are generally of first order, with the exception of the linear-to-zigzag phase transition which is known to be of second order [7–9]. As a symmetry breaking scenario, it provides a natural testing ground for universal dynamics of phase transitions and topological defect formation [9–12], recently explored in the laboratory [13–16].

Another fundamental setting in nonequilibrium statistical mechanics considers the thermal transport in low-dimensional systems, which exhibits a rich variety of anomalous features, including the breakdown of Fourier's law of heat conduction, instances in which subdiffusive and superdiffusive behavior can be observed [17–19], as well as the divergence of the thermal conductivity with the system size [20,21]. Most rigorous theoretical results have been obtained for exactly solvable quasifree models while systems with nonlinearities are typically exceedingly difficult to treat. Equally, the controlled generation of nonlinear physics in mesoscopic ion crystals is nontrivial and much recent progress has concerned harmonic models of complex networks and trapped-ion chains [22–24]. The richest phenomenology, however, can be expected in nonintegrable models [25] which mandates the development of both theoretical and experimental methods for their examination.

In this work, we advance further the case for trapped ions as a model system for the examination of challenging problems in mesoscopic physics by considering continuously driven ion chains between two thermal reservoirs as a platform in which to explore heat transport across an ion Coulomb crystal that experiences a structural phase transition.

We describe a realistic experimental configuration which is quite reminiscent of the lattice models extensively studied in an attempt to provide a rigorous derivation of Fourier's law from a microscopic Hamiltonian description [20,21]. While most theoretical studies have focused on one-dimensional chains of oscillators with nearest-neighbor interactions, we are dealing with a model system including both the external substrate potential of the trap, and the full Coulomb interparticle interaction. The interplay between these two terms, which can be experimentally controlled by changing the trapping frequencies, leads to a rich dynamics that ranges from the very stable linear confinements to the strong instabilities arising in the phase transitions.

We will show that the quasilinear configurations exhibit a dynamics dictated by the trapping potential, and therefore their transport properties resemble that of homogeneous harmonic chains [20,21]. As the ion chain crosses the transition from the linear to zigzag phase, the increasing role of the Coulomb interaction induces both significant nonlinearities and axial-transverse mode coupling which can lead to qualitative changes in both the local temperature profile and the total heat flux through the chain that may be observed experimentally.

The paper is organized in the following way. In Sec. II we introduce a model to describe the system dynamics. Section III provides a discrete approach to define the heat flux and the local kinetic temperature across the ion chain in terms of dynamical variables. In Sec. IV we fix the model parameters according to a realistic experimental setup and present the numerical results. We analyze the local temperature and the total heat flux in the proximity of the linear-to-zigzag phase transition, as a function of the trap frequency ratio. A spectral

analysis of the steady evolution of the coordinates of the inner ions in the chain is also presented. Sec. V puts together the main conclusions of this paper.

II. THE SYSTEM DYNAMICS

We consider an effectively two-dimensional system composed of N ions of mass m, charge Q, positions $\mathbf{q}_n = (q_{x,n}, q_{y,n})$ and momenta $\mathbf{p}_n = (p_{x,n}, p_{y,n})$, with $n = 1, \ldots, N$, which are confined in a trap with axial frequency ν along the x axis and transverse frequency ν_t along the y axis. The Hamiltonian of the system can be written as

$$H = \frac{1}{2m}\sum_{n=1}^{N}\left(p_{x,n}^2 + p_{y,n}^2\right) + \mathcal{V}. \tag{1}$$

The interaction potential $\mathcal{V}$ accounts for both the harmonic trap and the Coulomb repulsion, and is given by

$$\mathcal{V} = \frac{m}{2}\sum_{n=1}^{N}\left(\nu^2 q_{x,n}^2 + \nu_t^2 q_{y,n}^2\right) + \frac{1}{2}\left(\frac{Q^2}{4\pi\varepsilon_0}\right)\sum_{n=1}^{N}\sum_{l\neq n}^{N}\frac{1}{|\mathbf{q}_n - \mathbf{q}_l|}. \tag{2}$$

A quasilinear confinement of the ions along the x axis can be achieved by considering a strongly anisotropic trap, with $\nu_t \gg \nu$. We note that, at variance with lattice systems, none of the ions are pinned, which allows for an intricate interplay between axial and radial modes of motion.

We assume that the dynamics due to the external Doppler cooling lasers acting on the ions can be modeled as Langevin thermostats. This together with the typical separations between the ions (generally of the order of microns) justifies an intrinsically noisy classical description of the dynamics,

$$dq_{\mu,n} = \frac{p_{\mu,n}}{m}\,dt,$$
$$dp_{\mu,n} = -\left(\frac{\partial\mathcal{V}}{\partial q_{\mu,n}} + \frac{\eta_{\mu,n}}{m}\,p_{\mu,n}\right)dt + \sqrt{2\,D_{\mu,n}}\,dW_{\mu,n}, \tag{3}$$

where $\eta_{\mu,n}$ and $D_{\mu,n}$ are the friction and diffusion coefficients, respectively, $dW_{\mu,n}$ denote the Wiener processes resulting from the Gaussian white-noise forces $\varepsilon_{\mu,n}(t)$ associated with the interaction with the laser beams, which satisfy $\langle\varepsilon_{\mu,n}(t)\rangle = 0$ and $\langle\varepsilon_{\mu,n}(t)\,\varepsilon_{\mu,n}(t')\rangle = 2\,D_{\mu,n}\,\delta(t-t')$, and $\mu = (x,y)$.

For small laser intensities the friction and diffusion coefficients can be obtained from the Doppler cooling expressions [26]

$$\eta_{\mu,n} = -4\hbar k_{\mu,n}^2\left(\frac{I_{\mu,n}}{I_0}\right)\frac{(2\delta_{\mu,n}/\Gamma)}{[1+4\delta_{\mu,n}^2/\Gamma^2]^2},$$
$$D_{\mu,n} = \hbar^2 k_{\mu,n}^2\left(\frac{I_{\mu,n}}{I_0}\right)\frac{\Gamma}{\left[1+4\delta_{\mu,n}^2/\Gamma^2\right]}, \tag{4}$$

where $I_{\mu,n}/I_0$ is the normalized intensity of the laser beam acting on the n ion along the μ direction, $k_{\mu,n}$ is the corresponding laser wavelength, $\delta_{\mu,n} = \omega_{\mu,n} - \omega_0$ is the detuning of the laser frequency $\omega_{\mu,n}$ with respect to the frequency ω_0 of a selected atomic transition in the ions, and Γ is the natural linewidth of the excited state in such a transition.

The analysis of the system dynamics can be simplified considering dimensionless variables that lead to a single parameter interaction potential $\mathcal{V}$, determined by the ratio of the trap frequencies $\alpha = \nu_t/\nu$; see Appendix A.

III. HEAT FLUX AND LOCAL KINETIC TEMPERATURE

A discrete definition of the heat current through the chain can be obtained from the local energy density associated with each ion [20,21], which can be written as

$$h_n = \frac{1}{2m}\left(p_{x,n}^2 + p_{y,n}^2\right) + V(\mathbf{q}_n) + \frac{1}{2}\sum_{l\neq n}^{N}U(|\mathbf{q}_l - \mathbf{q}_n|), \tag{5}$$

where V represents the harmonic trap and U the Coulomb term of the interaction potential $\mathcal{V}$ given in Eq. (2). The time derivative of h_n leads to the discrete continuity equations

$$\frac{dh_n}{dt} = \sum_{l<n}^{N} j_{n,l} - \sum_{l>n}^{N} j_{l,n} + j_{B,n}, \tag{6}$$

where

$$j_{n,l} = -\frac{1}{2m}\sum_{\mu=\{x,y\}}\frac{\partial U(|\mathbf{q}_l - \mathbf{q}_n|)}{\partial q_{\mu,n}}\left(p_{\mu,n} + p_{\mu,l}\right) \tag{7}$$

can be identified as the energy current from the l ion to the n ion. For the n ion, the first term in Eq. (6) corresponds to the total energy current coming from the ions on the left, whereas the second term is the total energy current going to the ions on the right; see Fig. 1.

The last term

$$j_{B,n} = \sum_{\mu=\{x,y\}}\frac{p_{\mu,n}}{m}\left(-\frac{\eta_{\mu,n}}{m}\,p_{\mu,n} + \varepsilon_{\mu,n}\right) \tag{8}$$

is the energy current from the laser reservoirs.

The steady-state average of Eq. (6) implies the balance

$$\sum_{l<n}^{N}\langle j_{n,l}\rangle + \langle j_{B,n}\rangle = \sum_{l>n}^{N}\langle j_{l,n}\rangle \tag{9}$$

between the average rate at which each ion receives energy from the ions on the left and the laser beams, and the average rate at which such ion transfers energy to the ions on the right. The average of the energy currents from the reservoirs can be obtained using Novikov's theorem [27],

$$\langle j_{B,n}\rangle = \frac{1}{m^2}\sum_{\mu=\{x,y\}}\left(-\eta_{\mu,n}\langle p_{\mu,n}^2\rangle + m\,D_{\mu,n}\right). \tag{10}$$

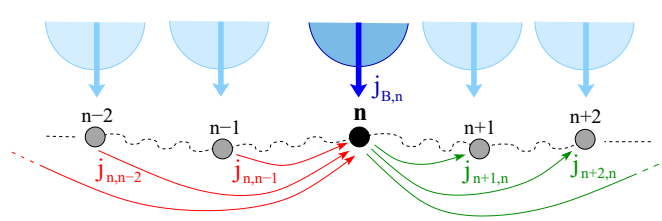

FIG. 1. (Color online) An illustration of some of the energy currents associated with the n ion in the chain.

The total heat current can be derived from a discrete description of the continuity equation [20,21]

$$\frac{\partial}{\partial t}h(\mathbf{q},t) + \nabla\cdot\mathbf{j}(\mathbf{q},t) = \sum_{n=1}^{N} j_{B,n}(t)\delta(\mathbf{q}-\mathbf{q}_n), \tag{11}$$

by taking the energy and heat flux densities as

$$h(\mathbf{q},t) = \sum_{n=1}^{N} h_n(t)\delta(\mathbf{q}-\mathbf{q}_n), \quad \mathbf{j}(\mathbf{q},t) = \sum_{n=1}^{N} \mathbf{j}_n(t)\delta(\mathbf{q}-\mathbf{q}_n), \tag{12}$$

respectively, with h_n being the local energy density defined in Eq. (5) and $\mathbf{j}_n$ the local flux. A Fourier analysis of Eq. (11) leads to

$$\mathbf{j}_n(t) = \mathbf{q}_n\left(\frac{dh_n}{dt} - j_{B,n}\right) + h_n\frac{d\mathbf{q}_n}{dt}. \tag{13}$$

Then the total heat flux, obtained by integration of the flux density over the chain volume, reads

$$\mathbf{J}(t) = \frac{1}{m}\sum_{n=1}^{N} h_n\mathbf{p}_n + \sum_{n=1}^{N-1}\sum_{l=1}^{n}(\mathbf{q}_{n+1}-\mathbf{q}_l)j_{n+1,l}. \tag{14}$$

In the steady state, the averaged total heat flux is determined by just the local fluxes coming from the reservoirs, and applying Novikov's theorem [27] it follows that

$$\begin{aligned}\langle\mathbf{J}\rangle &= -\sum_{n=1}^{N}\langle\mathbf{q}_n j_{B,n}\rangle \\ &= \frac{1}{m^2}\sum_{n=1}^{N}\sum_{\mu=\{x,y\}}\left(\eta_{\mu,n}\langle p_{\mu,n}^2\mathbf{q}_n\rangle - m\,D_{\mu,n}\,\langle\mathbf{q}_n\rangle\right).\end{aligned} \tag{15}$$

The local kinetic temperature T_n of each ion can also be expressed in terms of discrete dynamical variables as

$$T_n = \frac{1}{2mk_B}\sum_{\mu=\{x,y\}}\left\langle p_{\mu,n}^2\right\rangle_\varepsilon \tag{16}$$

where $\langle\cdot\rangle_\varepsilon$ indicates the average over an ensemble of stochastic trajectories.

IV. NUMERICAL EXPERIMENTS

We consider a chain composed of N ions and analyze the response of the local temperature and the total heat flux to the phase transition from a quasi-linear to the planar zigzag spatial configuration as the transverse frequency of the trap is lowered. We consider a chain of $^{24}Mg^+$ ions, with $N = 30$, and fix an axial frequency of the trap to $\nu = 2\pi \times 50$ kHz. We study the dynamics for different transverse frequencies $\nu_t = \alpha\nu$.

An analysis of the static properties of the ion chain in the thermodynamic limit provides an estimate of the local value of the critical ratio of the trap frequencies leading to the phase transition between the linear and the zigzag configurations [9],

$$\alpha_c(x) = \sqrt{\frac{7\zeta(3)}{2m\nu^2}\left(\frac{Q^2}{4\pi\varepsilon_0}\right)}\,[n(x)]^{3/2}, \tag{17}$$

where ζ is the Riemann-zeta function, and $n(x) = (3N/4L)[1-(x/L)^2]$ is the equilibrium linear density of ions along the trap axis as a function of distance x from the chain's center and the half-length of the chain L [28]. Due to the axial harmonic confinement the center of the chain experiences a higher axial density and Coulomb repulsion, making the phase transition spatially inhomogeneous.

In our numerical studies we assume that the ions are initially at rest and arranged with random positions in the close vicinity of the linear configuration. Then the reservoir lasers that act on the selected ions are switched on instantaneously. To determine the friction and the diffusion coefficients that characterize the interaction of the $^{24}Mg^+$ ions with the laser beams, we have applied the Doppler cooling expressions (4) to the atomic transition $3s^2S_{1/2} \longrightarrow 3p^2P_{1/2}$ with frequency $\omega_0 = 2\pi \times 1069$ THz [29] and an excited state natural linewidth $\Gamma = 2\pi \times 41.296$ MHz [30]. Given these values, the interaction of a laser beam with an ion is a function of the normalized intensity $I_{\mu,n}/I_0$ and the detuning $\delta_{\mu,n}$.

To drive a heat current through the chain, the ions at opposite ends of the ion crystal are subjected to different laser beams. In particular, we consider that the three leftmost (rightmost) ions interact with laser beams with normalized intensity $I_L = I_{\mu,n}/I_0 = 0.08$ ($I_R = I_L$) and detuning $\delta_L = \delta_{\mu,n} = -0.02\Gamma$ ($\delta_R = \delta_{\mu,n} = -0.1\Gamma$), with $n = 1,2,3$ ($n = N-2, N-1, N$). The different detunings δ_L and δ_R lead to effective reservoirs operating at different temperatures on both ends of the chain, and therefore a stationary nonequilibrium heat current. We assume that no laser beams are acting on the inner ions, corresponding to $n = 4,\ldots,N-3$.

We are principally concerned with the steady state behavior of the system. As a criterion to determine that the system has reached such a state we verify expression (9) for each ion, and also apply equality (15) to the whole chain. Appendices B and C provide details of the numerical integration and the characteristic timescales involved in the nonequilibrium dynamics towards the steady state. Note that in order to avoid excessively small time steps the numerical model neglects micromotion. While this represents a significant approximation in the zigzag configuration of an ion Coulomb crystal in a rf-Paul trap, it should be noted, however, that micromotion is absent in Penning traps in which analogous structural phase transitions were recently observed and Doppler cooling can be implemented [31].

As Fig. 2 shows, the temperature profile adopts a gradient along the chain which progressively increases as the transverse frequency of the trap is reduced to drive the transition from the linear to the zigzag spatial distributions. The numerical simulations indicate that the phase transition first emerges for $\alpha_c(0) \simeq 11.6$. For $\alpha > \alpha_c(0)$ the chain is fully linear and the temperatures T_n ($n = 4,\ldots,N-3$) of the inner ions tend to settle on a constant value for all n, which for this system is close to the mean temperature $(T_1+T_N)/2$ that is expected in a homogeneous harmonic chain with nearest-neighbor interactions [32], despite the presence of the axial quadratic potential [33]. Indeed, a spectral analysis of the steady evolution of the coordinates of the inner ions in linear chains indicates that their axial dynamics is close to the Brownian motion of a simple harmonic oscillator with characteristic frequency ν. Figure 3 illustrates that the power

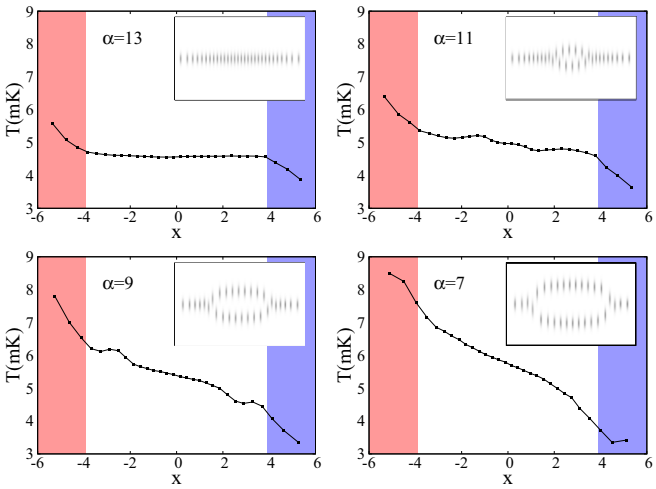

FIG. 2. (Color online) The local temperature profiles along the ion chain vs the distance x from the chain's center, for different ratios of the trap frequencies α. The lines between points are drawn to guide the eye. The insets show the corresponding steady ion distribution obtained from a single stochastic trajectory. The color boxes indicate the ions that are connected to the laser beams.

spectra of these ions are dominated by a well defined single peak corresponding to the axial trap frequency. Also an ordered series of much less intense peaks corresponding to higher order multiples of ν can be distinguished. The much lower intensity of the transverse spectrum evidences the minor role of this mode, due to the strong trap confinement in the transverse direction.

The simple axial spectrum observed in the linear chains corroborates the expectation that a harmonic approximation to the system Hamiltonian is valid; the system is effectively integrable, and the heat carriers are freely propagating phonons. The lack of temperature gradient is characteristic of this ballistic behavior.

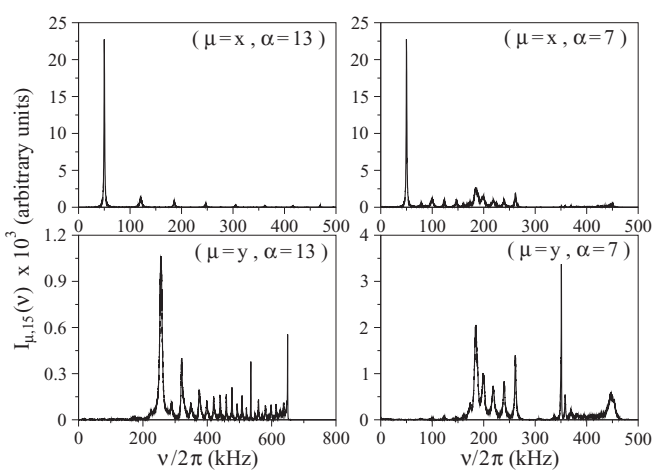

FIG. 3. Power spectra of the axial and the transverse motions for the central ion in a linear chain ($\alpha = 13$) and in a chain with zig-zag spatial distribution ($\alpha = 7$), see Fig. 2. See Appendix D for more details on the power spectra.

This situation is expected to change when the chain approaches the structural phase transition at $\alpha_c(0)$ where the chain buckles with the growth of the zigzag soft mode. Near this point nonlinearities as well as mode coupling between axial and radial modes play an increasing role and the harmonic chain description is expected to fail. While the nonlinearities lead to scattering, the axial-radial mode coupling leads to an effective dynamics akin to dephasing noise. Both effects, if significant, are known to contribute to the formation of a temperature gradient in the chain. It should be noted that nonlinearities tend to be relatively small unless the chain is very close to the phase transition point [34]. Hence we expect coupling between radial and axial modes to dominate. The deviations from the harmonic picture are also witnessed by the power spectra of the axial motion of the ions in the zigzag configuration, which exhibit continuous distributions of peaks that were not present in the linear chains; see Fig. 3. This emerging broadband nature of the spectra can be assigned to the axial-transverse mode coupling, which already occurs in the absence of the laser reservoirs; see Appendix D.

As the harmonic chain description ceases to be valid, the heat transport through the chain is modified, as evidenced by the emergence of a temperature gradient, signaling that an effective anomalous size-dependent heat conductivity could be formally introduced.

In addition to the emergence of Fourier's law when approaching the structural phase transition, one may also observe clear signatures of the structural phase transition in the heat flux across the chain, as shown in Fig. 4. Initially, on approaching the structural phase transition from the linear chain, one observes a progressive increase of the heat flux. This has two origins. Firstly, in the proximity of the transition the transverse modes will start to contribute to transport. Secondly, the increased thermal motion of the ions as the chain softens upon approach of the phase transition lead to an increased level of fluctuations. This noise may assist transport

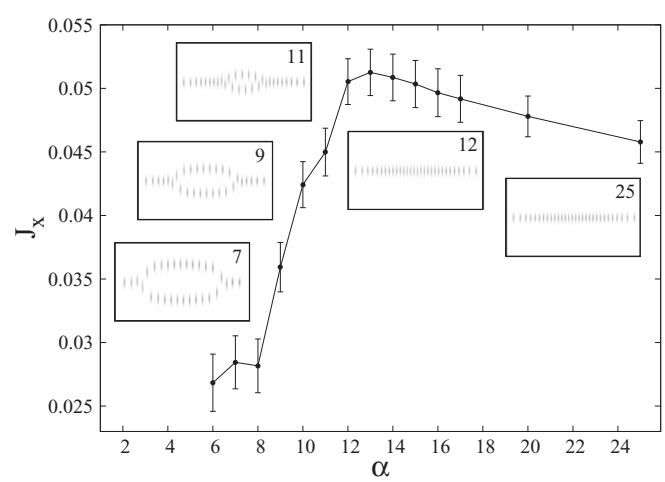

FIG. 4. Total heat flux in the axial direction as a function of the trap frequency ratio α. The error bars provide a measure of the fluctuations around the steady-state ensemble-average, and have been obtained according to (average)±(standard deviation). The maximum heat transport is achieved in the high-symmetry (linear) phase in the proximity of the critical point, with $\alpha \approx 13$.

as it overcomes the effects of spatial inhomogeneity in the chain [35]. Upon further decrease of α the chain buckles, leading to two possible heat conduction paths, while the inter-ion distances increase which in turn leads to a reduction in the interaction between neighboring ions and therefore a reduction of the heat flux. While initially, close to the phase transition, the increase in distance is compensated for by the formation of two independent channels, deeper in the zigzag configuration this is not the case anymore and the heat flux reduces.

Before closing we point out that a thermal conductance could be estimated from the temperature gradient and the axial heat flux measured in a nonequilibrium steady state. The spatial constraints imposed by the finite size and low-dimensionality of trapped-ion chains prompt the analysis of the thermal conductance as a function of the length, instead of a size-independent thermal conductivity of interest in a macroscopic model of thermal conduction. An alternative approach to obtain the heat conductance of a specific ion chain could be based on Green-Kubo type linear response expressions valid for the heat current in finite low-dimensional systems coupled to heat reservoirs [21,36].

V. CONCLUSIONS

Our analysis based on the local temperature profile and the total heat flux indicates that trapped-ion chains exhibit anomalous heat transport. The linearly distributed ions resemble harmonic chains, and therefore an integrable system, in which the free energy transport along the chain by noninteracting axial modes precludes the establishment of a temperature gradient and would lead to a divergent thermal conductivity. The phase transition from the linear to the bidimensional zigzag configuration induces a coupling between axial and transverse modes that hinders the transport of energy along the chain, and allows the emergence of a central domain in which a temperature gradient can be set up. Such domain grows as the transverse frequency is lowered and the bidimensional configuration extends towards the ends of the chain, resulting in a significant decrease of the axial heat flux. Heat transport is optimal in the linear configuration in the proximity of the critical point.

Note added: After the completion of this work, we learned about Ref. [37] devoted to the study of quantum heat conduction in harmonic ion chains. Some of their results, from the analysis of heat transport as a function of the crystal structure and a numerically introduced measure of disorder, are in good correspondence with our discussion about the relevance of nonlinearities and the axial-transverse mode coupling effects in the proximity of the linear-to-zigzag phase transition. In particular, the linear temperature profile and the remarkable insulating behavior observed in the artificially disordered two-dimensional harmonic configuration naturally arise from our intrinsic nonlinear approach that fully takes into account the many-body Coulomb interaction. Also, both models show the lack of temperature gradient that evidences the breakdown of the Fourier's law in the quasiharmonic linear chains.

ACKNOWLEDGMENTS

It is a pleasure to acknowledge discussions with H. Häffner, T. E. Mehlstäubler, J. P. Palao, J. M. Plata and D. Roy. We thank A. Muñoz for access to his computer facilities. This project was funded by the Spanish MICINN, the European Union (FEDER) (FIS2010-19998), the EU Integrating project SIQS, the EU STREP EQUAM, the Alexander von Humboldt Professorship (M.B.P.) and the U.S. Department of Energy through the LANL/LDRD Program and a LANL J. Robert Oppenheimer Fellowship (AdC).

APPENDIX A: DIMENSIONLESS VARIABLES

To define the dimensionless variables we start by introducing a characteristic system length ℓ, given by the relation

$$\ell^3 = \frac{1}{m\nu^2}\left(\frac{Q^2}{4\pi\varepsilon_0}\right). \tag{A1}$$

Defining the dimensionless ion coordinate and momentum vectors as

$$\tilde{\mathbf{q}}_n = (\tilde{q}_{x,n}, \tilde{q}_{y,n}) = \left(\frac{q_{x,n}}{\ell}, \frac{q_{y,n}}{\ell}\right) \tag{A2}$$

and

$$\tilde{\mathbf{p}}_n = (\tilde{p}_{x,n}, \tilde{p}_{y,n}) = \left(\frac{p_{x,n}}{\ell m\nu}, \frac{p_{y,n}}{\ell m\nu}\right), \tag{A3}$$

and the one-parameter dimensionless interaction potential

$$\tilde{\mathcal{V}} = \frac{\mathcal{V}}{\ell^2 m\nu^2} = \frac{1}{2}\sum_{n=1}^{N}\left(\tilde{q}_{x,n}^2 + \alpha^2\,\tilde{q}_{y,n}^2\right) + \frac{1}{2}\sum_{n=1}^{N}\sum_{l\neq n}^{N}\frac{1}{|\tilde{\mathbf{q}}_n - \tilde{\mathbf{q}}_l|}, \tag{A4}$$

where $\alpha = \nu_t/\nu$ is the aspect ratio of the trap frequencies, the equations of motions (3) take the form

$$d\tilde{q}_{\mu,n} = \tilde{p}_{\mu,n}\,d\tilde{t},$$
$$d\tilde{p}_{\mu,n} = -\left(\frac{\partial\tilde{\mathcal{V}}}{\partial\tilde{q}_{\mu,n}} + \tilde{\eta}_{\mu,n}\,\tilde{p}_{\mu,n}\right)d\tilde{t} + \sqrt{2\,\tilde{D}_{\mu,n}}\;d\tilde{W}_n, \tag{A5}$$

with the dimensionless time

$$\tilde{t} = \nu t, \tag{A6}$$

the Wiener processes

$$d\tilde{W}_{\mu,n} = \sqrt{\nu}\,dW_{\mu,n}, \tag{A7}$$

the friction coefficients

$$\tilde{\eta}_{\mu,n} = \frac{\eta_{\mu,n}}{m\nu}, \tag{A8}$$

and the diffusion coefficients

$$\tilde{D}_{\mu,n} = \frac{D_{\mu,n}}{\ell^2 m^2\nu^3}. \tag{A9}$$

In terms of the dimensionless variables, the total heat flux (14) is expressed as

$$\tilde{\mathbf{J}} = \frac{\mathbf{J}}{\ell^3 m\nu^3} = \sum_{n=1}^{N}\tilde{h}_n\tilde{\mathbf{p}}_n + \sum_{n=1}^{N-1}\sum_{l=1}^{n}(\tilde{\mathbf{q}}_{n+1} - \tilde{\mathbf{q}}_l)\,\tilde{j}_{n+1,l}, \tag{A10}$$

with the dimensionless local energy densities and currents

$$\tilde{h}_n = \frac{h_n}{\ell^2 m \nu^2} \tag{A11}$$

and

$$\tilde{j}_{l,n} = \frac{j_{l,n}}{\ell^2 m \nu^3}, \tag{A12}$$

respectively. The dimensionless local temperatures are given by

$$\tilde{T}_n = \left(\frac{k_B}{\ell^2 m \nu^2}\right) T_n = \frac{1}{2} \sum_{\mu=\{x,y\}} \langle \tilde{p}^2_{\mu,n} \rangle_\varepsilon. \tag{A13}$$

In the next section we will continue the analysis in terms of the dimensionless variables. We will remove the tilde symbol from all the variables and parameters to simplify the notation.

APPENDIX B: THE NUMERICAL INTEGRATION

The $4N$-dimensional stochastic differential equations (A5) can be expressed in a compact form as

$$d\mathbf{Y} = \mathbf{A}(\mathbf{Y})\, dt + \mathbf{B} \cdot d\mathbf{\Omega}_t, \tag{B1}$$

where the components of the variable vector $\mathbf{Y}$ have been ordered in the form

$$\mathbf{Y} = (q_{x,1}, \ldots, q_{x,N}, q_{y,1}, \ldots, q_{y,N}, p_{x,1}, \ldots p_{x,N}, p_{y,1}, \ldots, p_{y,N}). \tag{B2}$$

The components of the vector $\mathbf{A}$ containing the deterministic terms in the equations of motion are

$$A_i = \begin{cases} p_{x,i}, & i = 1, \ldots, N, \\ p_{y,i-N}, & i = N+1, \ldots, 2N, \\ -\left(\frac{\partial \mathcal{V}}{\partial q_{x,i-2N}} + \eta_{x,i-2N}\, p_{x,i-2N}\right), & i = 2N+1, \ldots, 3N, \\ -\left(\frac{\partial \mathcal{V}}{\partial q_{y,i-3N}} + \eta_{y,i-3N}\, p_{y,i-3N}\right), & i = 3N+1, \ldots, 4N. \end{cases}$$

The matrix $\mathbf{B}$ contains the diffusion coefficients $D_{\mu,n}$. In our model it can be expressed by a diagonal matrix with the elements

$$B_{ii} = \begin{cases} 0, & i = 1, \ldots, N, \\ 0, & i = N+1, \ldots, 2N, \\ \sqrt{2\, D_{x,i-2N}}, & i = 2N+1, \ldots, 3N, \\ \sqrt{2\, D_{y,i-3N}}, & i = 3N+1, \ldots, 4N. \end{cases} \tag{B3}$$

The vector $d\mathbf{\Omega}_t$ denotes the $4N$-dimensional Wiener process, whose elements are

$$d\Omega_{t,i} = \begin{cases} 0, & i = 1, \ldots, 2N, \\ dW_{i-2N}, & i = 2N+1, \ldots, 3N, \\ dW_{i-3N}, & i = 3N+1, \ldots, 4N. \end{cases} \tag{B4}$$

To integrate the stochastic differential equations (B1) we consider the multidimensional explicit order 2.0 weak scheme proposed by Platen [38]. Since in our model the matrix $\mathbf{B}$ does not depend explicitly on the variable $\mathbf{Y}$, such a scheme is particularly simple. Given the variable $\mathbf{Y}_I$ at a time step I, its value at the following time step $I+1$ is given by

$$\mathbf{Y}_{I+1} = \mathbf{Y}_I + \frac{1}{2}[\mathbf{A}(\mathbf{\Gamma}_I) + \mathbf{A}(\mathbf{Y}_I)]\Delta_t + \mathbf{B} \cdot \Delta\mathbf{\Omega}_I \tag{B5}$$

where

$$\mathbf{\Gamma}_I = \mathbf{Y}_I + \mathbf{A}(\mathbf{Y}_I)\Delta_t + \mathbf{B} \cdot \Delta\mathbf{\Omega}_I, \tag{B6}$$

$\Delta_t = t_{I+1} - t_I$ is the constant time interval between two consecutive time steps, and $\mathbf{\Omega}_I$ is the vector with elements

$$\Delta\Omega_{I,i} = \begin{cases} 0, & i = 1, \ldots, 2N, \\ \sqrt{\Delta_t}\; G_{I,x,i-2N}, & i = 2N+1, \ldots, 3N, \\ \sqrt{\Delta_t}\; G_{I,y,i-3N}, & i = 3N+1, \ldots, 4N, \end{cases} \tag{B7}$$

with $G_{I,\mu,n} \sim N(0;1)$ (standard Gaussian) a normally distributed random variable selected at time step I for the n ion, along the μ direction.

In order to get stable local temperatures and a total heat flux from the solutions of Eqs. (B1), numerical simulations were performed considering time intervals $\Delta_t < 1 \times 10^{-4}$, and integrated up to a final time in which the steady conditions (9) and (15) were satisfied. The process became computationally expensive as the multiple interaction potential (A4) had to be evaluated more than 4×10^7 times for each stochastic, and averages that included over 500 of these trajectories were considered. It took over two months to carry out the simulations and get stable results using a 32 CPU machine with AMD Opteron™ Processors 6134. The high cost of the classical simulations provides a further argument in support of the ion trap set up as an excellent (quantum) simulator for the analysis of energy transport in finite low-dimensional systems.

APPENDIX C: CHARACTERISTIC TIMESCALES IN THE NONEQUILIBRIUM DYNAMICS TOWARDS THE STEADY STATE

In the main text we present results obtained in terms of dynamical variables collected from long enough simulations for the system to reach a nonequilibrium steady state. In this section we indicate the characteristic timescales that are needed to achieve such a state, with associated time-independent local temperatures and heat fluxes. Figures 5 and 6 show some representative time evolutions of the local temperatures and the total heat fluxes towards the steady state configuration, obtained from an average over more than 800 stochastic trajectories. The ions at both ends of the chain that are directly connected to the laser beams reach steady values faster than the inner ions. The slowest convergence occurs for the central ions of the linear chain. In general, it can be assumed that the system stabilizes after approximately 5–10

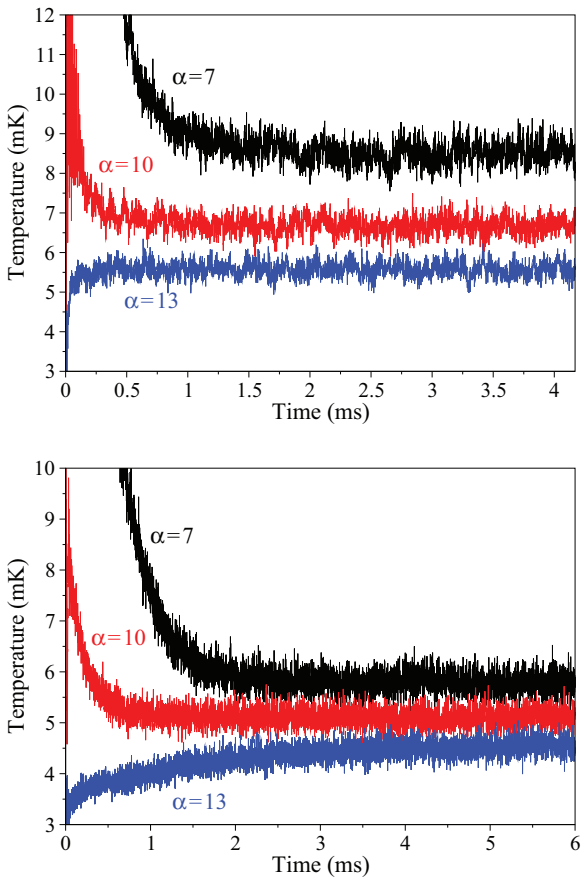

FIG. 5. (Color online) Time evolution of the local temperatures of the leftmost ion ($n = 1$, upper panel) and the central ion ($n = 15$, lower panel) for chains with different ratios of the trap frequencies.

ms. To ensure accurate temperature profiles and heat fluxes, the simulations have been performed up to 13 ms, and the final results have been obtained from a time average within the interval [10,13] ms.

Hence we are considering short-time-scale experiments in which effects such the motional heating of the trapped ions confined in rf traps due to fluctuating electric fields from the trap electrodes should not be relevant.

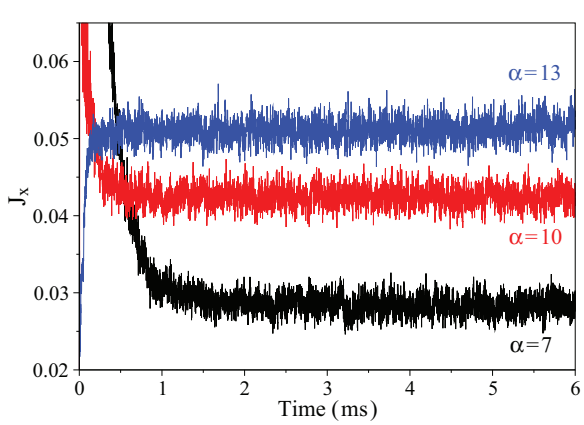

FIG. 6. (Color online) Time evolution of the total heat flux in the axial direction, obtained from Eq. (15) as the energy flow between the ions at the ends of the chain and the corresponding laser reservoirs.

APPENDIX D: POWER SPECTRA OF THE TRAPPED IONS

To get an insight into the dynamics of a given n ion in the chain, we have considered the power spectra obtained from the steady evolution of the axial ($q_{x,n}$) and transverse ($q_{y,n}$) coordinates, given by

$$I_{\mu,n}(\nu) = \frac{1}{\tau}\left\langle \left| \int_{t_s}^{t_s+\tau} dt\, e^{i\nu t}\, q_{\mu,n}(t) \right|^2 \right\rangle_{\varepsilon}, \qquad \text{(D1)}$$

where t_s is an arbitrary time value at the steady region and τ a long enough time interval. $\langle\cdot\rangle_{\varepsilon}$ denotes the average over an ensemble of stochastic trajectories. Experimentally, it can be measured using, e.g., the Ramsey scheme [39].

The appearance of the power spectra presented in the main text is conditioned by the interaction of the ion chain with the laser reservoirs. The identification of the spectral features associated with such interaction allows a more accurate analysis of the dynamics.

As Fig. 7 shows, the heat reservoirs cause a slight broadening of the distinct peaks associated with the trapping frequencies, whereas they do not introduce significant changes in the remaining spectral pattern. Therefore, the emergence of a continuous distribution of peaks in the proximity of the structural phase transition is intrinsic to the dynamics of the isolated chain of trapped ions.

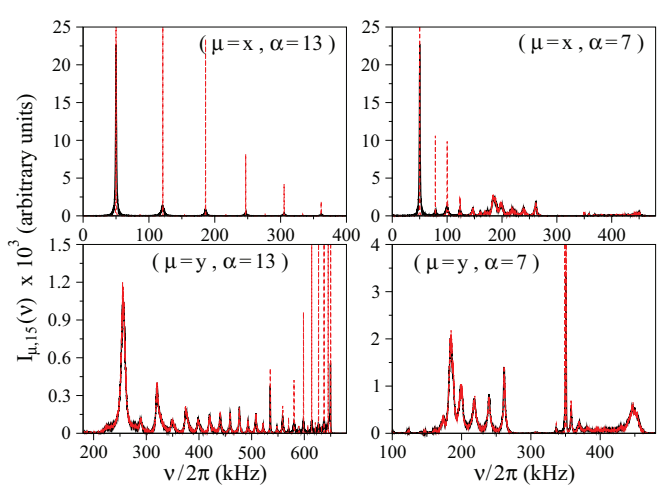

FIG. 7. (Color online) The power spectra of Fig. 3 in the main text (solid line) and the power spectra corresponding to the free evolving chain of trapped ions, after disconnecting the laser beams at time $t = t_s$ (red dashed line).

[1] H. Häffner, C. F. Roos, and R. Blatt, Phys. Rep. **469**, 155 (2008).
[2] C. Schneider, D. Porras, and T. Schaetz, Rep. Prog. Phys. **75**, 024401 (2012).
[3] R. Blatt and C. F. Roos, Nat. Phys. **8**, 277 (2012).
[4] G. Birkl, S. Kassner, and H. Walther, Nature (London) **357**, 310 (1992).
[5] I. Waki, S. Kassner, G. Birkl, and H. Walther, Phys. Rev. Lett. **68**, 2007 (1992).
[6] D. H. E. Dubin and T. M. O'Neil, Rev. Mod. Phys. **71**, 87 (1999).
[7] J. P. Schiffer, Phys. Rev. Lett. **70**, 818 (1993).
[8] G. Piacente, I. V. Schweigert, J. J. Betouras, and F. M. Peeters, Phys. Rev. B **69**, 045324 (2004).
[9] S. Fishman, G. De Chiara, T. Calarco, and G. Morigi, Phys. Rev. B **77**, 064111 (2008).
[10] A. Retzker, R. C. Thompson, D. M. Segal, and M. B. Plenio, Phys. Rev. Lett. **101**, 260504 (2008).
[11] A. del Campo, G. De Chiara, G. Morigi, M. B. Plenio, and A. Retzker, Phys. Rev. Lett. **105**, 075701 (2010).
[12] G. De Chiara, A. del Campo, G. Morigi, M. B. Plenio, and A. Retzker, New J. Phys. **12**, 115003 (2010).
[13] M. Mielenz, J. Brox, S. Kahra, G. Leschhorn, M. Albert, T. Schaetz, H. Landa, and B. Reznik, Phys. Rev. Lett. **110**, 133004 (2013).
[14] S. Ejtemaee and P. C. Haljan, Phys. Rev. A **87**, 051401(R) (2013).
[15] S. Ulm, J. Roßnagel, G. Jacob, C. Degünther, S. T. Dawkins, U. G. Poschinger, R. Nigmatullin, A. Retzker, M. B. Plenio, F. Schmidt-Kaler, and K. Singer, Nat. Commun. **4**, 2290 (2013).
[16] K. Pyka, J. Keller, H. L. Partner, R. Nigmatullin, T. Burgermeister, D. M. Meier, K. Kuhlmann, A. Retzker, M. B. Plenio, W. H. Zurek, A. del Campo, and T. E. Mehlstäubler, Nat. Commun. **4**, 2291 (2013).
[17] B. Li, L. Wang, and B. Hu, Phys. Rev. Lett. **88**, 223901 (2002)
[18] D. Alonso, A. Ruiz, and I. de Vega, Phys. Rev. E **66**, 066131 (2002).
[19] D. Alonso, A. Ruiz, and I. de Vega, Physica D **187**, 184 (2004).
[20] S. Lepri, R. Livi, and A. Politi, Phys. Rep. **377**, 1 (2003).
[21] A. Dhar, Adv. Phys. **57**, 457 (2008).
[22] E. A. Martinez and J. P. Paz, Phys. Rev. Lett. **110**, 130406 (2013).
[23] A. Bermudez, M. Bruderer, and M. B. Plenio, Phys. Rev. Lett. **111**, 040601 (2013).
[24] M. Ramm, T. Pruttivarasin, and H. Häffner, arXiv:1312.5786.
[25] B. Hu, B. Li, and H. Zhao, Phys. Rev. E **57**, 2992 (1998); **61**, 3828 (2000).
[26] See for example W. D. Phillips, in *Laser Manipulation of Atoms and Ions*, edited by E. Arimondo, W. D. Phillips, and F. Strumia, Proceedings of the International School of Physics "Enrico Fermi", Course CXVIII (North-Holland, Amsterdam, 1992), p. 289.
[27] E. A. Novikov, JETP **20**, 1290 (1965).
[28] D. H. E. Dubin, Phys. Rev. E **55**, 4017 (1997).
[29] The frequency was obtained from the energy transition $E_{eg} = E_e - E_g = 4.2243$ eV taken from the NIST Atomic Spectra Database 1999. http://physics.nist.gov
[30] W. Ansbacher, Y. Li, and E. H. Pinnington, Phys. Lett. A **139**, 165 (1989).
[31] S. Mavadia, J. F. Goddwin, G. Stutter, S. Bharadia, D. R. Crick, D. M. Segal, and R. C. Thompson, Nat. Commun. **4**, 2571 (2013).
[32] Z. Rieder, J. L. Lebowitz, and E. Lieb, J. Math. Phys. **8**, 1073 (1967).
[33] T. Prosen and D. K. Campbell, Chaos **15**, 015117 (2005). See Subsection II A 2.
[34] C. Marquet, F. Schmidt-Kaler, and D. F. V. James, Appl. Phys. B **76**, 199 (2003).
[35] M. B. Plenio and S. F. Huelga, New J. Phys. **10**, 113019 (2008).
[36] A. Kundu, A. Dhar, and O. Narayan, J. Stat. Mech. (2009) L03001.
[37] N. Freitas, E. Martinez, and J. P. Paz, arXiv:1312.6644.
[38] P. E. Kloeden and E. Platen, *Numerical Solution of Stochastic Differential Equations* (Springer, Berlin, 1999).
[39] G. De Chiara, T. Calarco, S. Fishman, and G. Morigi, Phys. Rev. A **78**, 043414 (2008).